NeuroImage 212 (2020) 116664

Contents lists available at ScienceDirect

NeuroImage

journal homepage: www.elsevier.com/locate/neuroimage

Orthonasal versus retronasal glomerular activity in rat olfactory bulb by fMRI

Basavaraju G. Sanganahalli [a,b,c,*], Keeley L. Baker [d,e], Garth J. Thompson [a,g], Peter Herman [a,b,c], Gordon M. Shepherd [d], Justus V. Verhagen [d,e], Fahmeed Hyder [a,b,c,f,**]

[a] Magnetic Resonance Research Center (MRRC), Yale University, New Haven, CT, USA
[b] Quantitative Neuroscience with Magnetic Resonance (QNMR) Core Center, Yale University, New Haven, CT, USA
[c] Department of Radiology and Biomedical Imaging, Yale University, New Haven, CT, USA
[d] Department of Neuroscience, Yale University, New Haven, CT, USA
[e] The John B. Pierce Laboratory, New Haven, CT, USA
[f] Department of Biomedical Engineering, Yale University, New Haven, CT, USA
[g] iHuman Institute, ShanghaiTech University, Shanghai, 201210, China

ARTICLE INFO

Keywords:
Retronasal
Orthonasal
Olfactory bulb
Glomeruli
fMRI

ABSTRACT

Odorants can reach olfactory receptor neurons (ORNs) by two routes: orthonasally, when volatiles enter the nasal cavity during inhalation/sniffing, and retronasally, when food volatiles released in the mouth pass into the nasal cavity during exhalation/eating. Previous work in humans has shown that both delivery routes of the same odorant can evoke distinct perceptions and patterns of neural responses in the brain. Each delivery route is known to influence specific responses across the dorsal region of the glomerular sheet in the olfactory bulb (OB), but spatial distributions across the entire glomerular sheet throughout the whole OB remain largely unexplored. We used functional MRI (fMRI) to measure and compare activations across the entire glomerular sheet in rat OB resulting from both orthonasal and retronasal stimulations of the same odors. We observed reproducible fMRI activation maps of the whole OB during both orthonasal and retronasal stimuli. However, retronasal stimuli required double the orthonasal odor concentration for similar response amplitudes. Regardless, both the magnitude and spatial extent of activity were larger during orthonasal versus retronasal stimuli for the same odor. Orthonasal and retronasal response patterns show overlap as well as some route-specific dominance. Orthonasal maps were dominant in dorsal-medial regions, whereas retronasal maps were dominant in caudal and lateral regions. These different whole OB encodings likely underlie differences in odor perception between these biologically important routes for odorants among mammals. These results establish the relationships between orthonasal and retronasal odor representations in the rat OB.

1. Introduction

Animals perceive their olfactory environment not only from odors originating in the external world (orthonasal route), but also from odors released in the oral cavity while eating food (retronasal route). These modes of chemical sensing serve important biological functions, e.g., from finding suitable mates to flavor perception. During retronasal olfaction, odorants can reach the olfactory receptor neurons (ORNs) in the nasal cavity when pulses of odor volatiles are released in the mouth through mastication or after swallowing and enter via the posterior nares of the nasopharynx (Buettner et al., 2001). This process differs from odors delivered orthonasally when volatile odorants enter the nasal cavity during inhalation or sniffing via the anterior nares. Both mice and rats are able to smell retronasally (Gautam and Verhagen, 2012a; Rebello et al., 2015) and retronasal odors can modify taste in rats (Gautam and Verhagen, 2010) and humans (Stevenson et al., 2004), probably involving the gustatory cortex (Blankenship et al., 2019; Samuelsen and Fontanini, 2017) as well as the olfactory cortex (Maier, 2017; Maier et al., 2012).

The route through which odorants are delivered to the olfactory epithelium affects perception, including intensity, in part based on delivery efficiency (Bojanowski and Hummel, 2012; Rozin, 1982).

* Corresponding author. Yale University, N143 TAC (MRRC), 300 Cedar Street, New Haven, CT, 06520, USA.
** Corresponding author. Yale University, N143 TAC (MRRC), 300 Cedar Street, New Haven, CT, 06520, USA.
E-mail addresses: basavaraju.ganganna@yale.edu (B.G. Sanganahalli), fahmeed.hyder@yale.edu (F. Hyder).

https://doi.org/10.1016/j.neuroimage.2020.116664
Received 8 October 2019; Received in revised form 22 January 2020; Accepted 16 February 2020
Available online 20 February 2020

Electroolfactogram recordings demonstrate longer response latencies of odors reaching olfactory receptors retronasally, even when total flow rate within the nasal cavity was the same (Scott et al., 2007a). Optical imaging of glomeruli in rodent olfactory bulb (OB) show that overall responses are lower and slower when the odorant is delivered retronasally compared to orthonasally (Furudono et al., 2013; Gautam and Verhagen, 2012b; Rebello et al., 2015; Scott et al., 2007a). Odor molecules being transported from the mouth to the nasal epithelium are subject to absorption along the walls of the oral and nasal cavities, a potential key determinant in odor discrimination (Kent et al., 2003). The odor polarity is a factor in the concentration that can reach the olfactory cleft, where polar odorants can reach lower concentrations (Frasnelli et al., 2005). Optical imaging has demonstrated that increasing odor polarity is associated with slower temporal responses in the dorsal OB (Gautam et al., 2014). Additionally, non-polar odors were observed to be more effective at retronasal stimulation than polar odors (Scott et al., 2007a, 2014).

The process that underlies the liberation of flavor from food is influenced by many factors. Temperature, hydration, surface area, enzymes, saliva, binding and phase inversion all contribute to the aroma release from food (Taylor and Roozen, 1996). The subsequent volatility of these compounds also contributes to differences in orthonasal and retronasal olfaction, where higher volatility of compounds enhances retronasal detection (Gautam and Verhagen, 2012b). Human studies have demonstrated that the retronasal route yields lower intensity than the orthonasal route (Pierce and Halpern, 1996). The process of flavor perception is in fact a highly multisensory process that encompasses touch, temperature, hearing and vision (Verhagen and Engelen, 2006). Human fMRI studies have highlighted that route of delivery influences differential regional activation which can subsequently be influenced by previous retronasal experiences (Small et al., 2005). Both spatial and temporal activations of glomeruli are key for odor discrimination (Li et al., 2014; Rebello et al., 2014; Shusterman et al., 2011; Smear et al., 2011; Spors and Grinvald, 2002; Spors et al., 2006). Optical imaging studies of the dorsal OB have highlighted that spatial patterns in glomerular responses based on orthonasal and retronasal odor delivery routes largely overlap, although fewer glomeruli respond to retronasal odors (Furudono et al., 2013; Gautam and Verhagen, 2012b; Rebello et al., 2015). Furthermore, like orthonasally delivered odors, increasing odor concentrations recruit more glomeruli when delivered retronasally as well as the response dynamics in the rat OB (Gautam et al., 2014).

Since optical imaging is spatially limited to a small dorsal region of the glomerular sheet, there is need for a methodical study of glomerular activity patterns of the entire OB. Previous studies have established that orthonasal fMRI response patterns can be localized to the glomerular layer in the entire OB for rat (Xu et al., 2000) and mouse (Xu et al., 2003). Here we build on our previous optical and fMRI studies to elucidate and compare spatiotemporal glomerular activity patterns of both orthonasal and retronasal olfaction in the entire OB.

2. Materials and methods

All procedures were performed in accordance with protocols approved by the Yale University School of Medicine Institutional Animal Care and Use Committee (IACUC) and Pierce Animal Care and Use Committee (PACUC). These procedures are in agreement with the National Institutes of Health Guide for the Care and Use of Laboratory Animals. The experiments in this study were aimed to compare orthonasal and retronasal odor stimuli in two separate animal groups.

2.1. Animal preparation

Sprague-Dawley rats (n = 6, for orthonasal; n = 5 for retronasal) weighing 250–300 g were purchased from Charles River Laboratories and housed individually in an environment of controlled humidity (60%) and temperature (23 °C). The vivarium was set with 12 h light-dark cycles and all the experiments were performed in the light phase. Rats were anesthetized with urethane (1.5 g/kg intraperitoneal), administered atropine to prevent nasal blockage (0.03 mg/kg, subcutaneous), and administered eye lubricant to prevent desiccation (Puralube Vet Ointment, ophthalmic ointment). Systemic physiology and rectal temperature were continuously monitored throughout the experiment. Temperature was maintained at ~37 °C using a water flow heating pad. Blood gas pH, pCO_2 and pO_2 were recorded once per hour. During orthonasal fMRI experiments rats were not intubated and were allowed to breathe freely throughout the experiment. Rats' head positions were fixed with ear bars and a bite bar in a cradle and placed under the surface coil. Through the nose-cone, compressed medical grade air was continuously given at 1000 mL/min, during baseline, and anatomical scans. For retronasal fMRI studies a double tracheotomy surgery was performed, allowing for the rat to sniff artificially. A Teflon tube (OD 2.1 mm, upper tracheotomy tube) was inserted 10 mm into the nasopharynx to assure that airflow was restricted to the nose (the epiglottis could otherwise leak air flow via the oral cavity). Another Teflon tube (OD 2.3 mm, lower tracheotomy tube) was inserted into the caudal end of the tracheal cut. Both tubes were fixed and sealed to the tissues using surgical thread and cyanoacrylate glue. The upper tracheotomy tube inserted into the nasopharynx was used to deliver odors retronasally. Local anesthetic (2% Lidocaine) was applied at all pressure points and incisions. This method was adapted from previous optical imaging retronasal studies (Gautam and Verhagen, 2012b). All imaging was done following anesthesia and surgery and animals were at no point allowed to awaken after these procedures.

2.2. Orthonasal and retronasal odorant presentation and odorants

Odors were delivered orthonasally and retronasally through a custom-built olfactometer with TTL-controlled solenoid valves (Cole-Parmer, Vernon Hills, IL), synchronized with an MRI acquisition computer. Detailed description of this device is reported elsewhere (Sanganahalli et al., 2009, 2016). The output flow (maintained at 1000 mL/min) was connected to a long (~4m) Teflon tube (ID: 2.24 mm) that was led into the scanner room and connected to a nose mask on the rat lying inside the magnet bore. The odor delivery delay due to the long tube was ~4 s. We have taken this time into account during the data processing. The state of each solenoid valve (open/closed) was switched using a relay circuit controlled by CED μ1401 unit (Cambridge Electronic Design Ltd., Cambridge, UK) using Spike2 software. Odor carrier N_2 was mixed with medical grade air flow to control the odor concentration. Odorant concentrations are indicated as percentage saturated vapor (% s.v.). Medical-grade air was used to dilute the vapor in the headspace of odorant reservoirs to generate the desired concentration. Odorants were diluted before reaching common tubing to maximize purity. The odor manifolds were automatically flushed with clean air after each stimulation cycle. We used an odor delivery nose cone mounted in the naso-incisor bite bar, which was an in-line wider extension of the Teflon tube from the olfactometer to ensure consistent odor delivery to both nares and fitted into the imaging bore of MRI scanner. Odor flowing from the 2.24 mm ID odor tube tends to be laminar and retain this diameter, and is hence likely to miss one or both nares, which is avoided by our wider extension as shown by flow models (Sanganahalli et al., 2016). Orthonasal odor delivery was precisely time-locked to fMRI acquisition in a block design experiment (0–30 s clean medical grade air, 30–89 s odor, 90–150 s clean medical grade air) and was controlled through Spike2 software. For retronasal odor delivery we used a novel bidirectional artificial sniffing paradigm and retronasal odor tube in double-tracheotomized rats. This procedure is copied form earlier studies (Gautam and Verhagen, 2012b). However, due to the necessary double tracheotomy, this precludes natural breathing through the nose and requires all-synthetic breathing including through a nose mask with excellent seal (Cf. Fig. 1 (Gautam and Verhagen, 2012b),). This is hard to achieve or assure in a rodent inside a MRI bore surrounded by RF coils. In addition, long olfactometer tubing is necessitated in the fMRI setting, which increases compliance and hence may differentially affect temporal

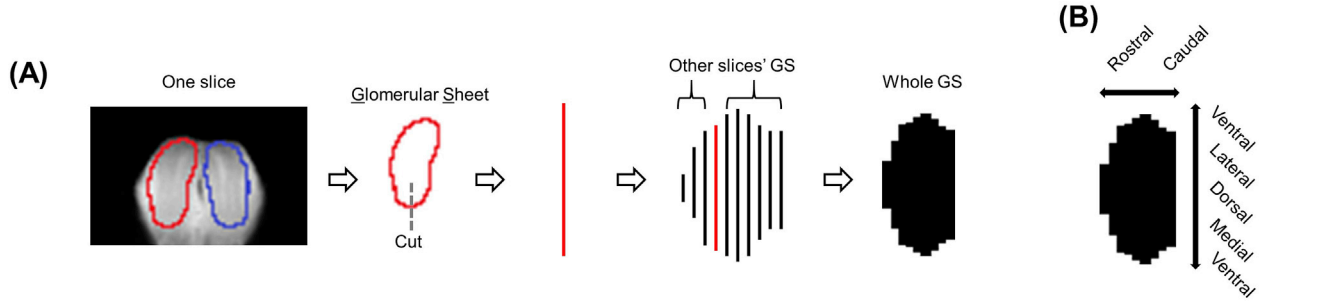

Fig. 1. (A) Process of converting 3D MRI data to a flatmap of the glomerular sheet (GS). The glomerular layer is traced on each coronal slice, the trace is cut at the bottom and flattened to a row, and then all such rows are combined to form the flatmap. Within each slice of the MRI data, the layer mask forms a ring shape, or an inverted-U shape. Thus, each row of the coronal image has either one or two sections of the layer in it. If there are two sections, these are the left and right sides of the layer. Arranging these voxels from left-bottom to left-top, concatenated with right-top to right-bottom converts the layer into a one-voxel row in the flatmap. As one row corresponds to one slice in the original MRI, combining all of the rows in slice order creates a flatmap. (B) Orientation of each flatmap. This flatmap will have a rostral-caudal dimension, assuming rows from coronal slices were concatenated. The other dimension will go ventral-medial-dorsal-lateral-ventral based on how it was unwrapped. Thus, a 2D image is produced of the layer. Code is provided in (Thompson et al., 2018).

patterning of the flow across the routes (as friction through the nose is route-dependent too), a parameter of no interest here. Retronasal odor delivery was precisely time-locked to fMRI acquisition in a block design experiment (3-min OFF, 2-min ON, 3-min OFF) and was controlled through Spike2 software. All the odorants were obtained from Sigma-Aldrich (St. Louis, MO, USA) and stored under nitrogen in the dark. To provide a continuous steady-state environment to the nasal mucosa, we applied humidified and preheated (28–30 °C) airflow between odor stimulations. Two different types of odorants were used in these experiments: ethyl butyrate (EB) and methyl valerate (MV). These monomolecular odorants were chosen from the family of odorants whose effects on the OB have been previously characterized (Johnson and Leon, 2000a,b; Sanganahalli et al., 2016; Uchida et al., 2000; Wachowiak and Cohen, 2001).

2.3. Data acquisition

Data were recorded on a 9.4T Bruker horizontal-bore spectrometer using a home-built ^{1}H surface coil radiofrequency probe (1.4 cm diameter). The whole OB was shimmed using the B0DETOX software (Juchem and de Graaf, 2017; Juchem et al., 2014). The static field inhomogeneity was optimized until the half-height line width of water in the shimming voxel was less than 15–20 Hz. The odor-evoked fMRI protocol was adapted from our earlier work (Kida et al., 2002; Sanganahalli et al., 2009, 2016; Xu et al., 2000).

For orthonasal studies we obtained fMRI data with single-shot gradient-echo EPI images (recycle time (TR) 1000 ms, echo time (TE) 15 ms, 64 × 32 matrix, 16 × 8 mm field-of-view (FOV), 16 dummy scans, 0.5 mm coronal slices, 10 slices) during rest (0–29s) odor (30–89s) rest (90–150s) epochs at 1 Hz. Parts of these data were partially published previously in Thompson et al., 2018. For retronasal studies we collected we obtained fMRI data with fast low-angle single shot (FLASH) gradient-echo imagining sequences with (FOV 1.4 cm^2; image matrix of 64 × 64; slice thickness of 250 μm; flip angle of 15–30°; TR 500 ms, and TE 15 ms; and voxel size of 220 × 220 × 250 μm^3. Temporal resolution was 20s for entire OB mapping. Sixteen dummy scans were carried out before fMRI data acquisition. Experiments were of a standard block design in which twenty-four scans of twenty slices consisted of nine pure air scans, six odor scans, and nine pure air scans. In all cases, experimental trials were separated by a recovery period of at least 15 min, a duration sufficient for >90% recovery (Schafer et al., 2006).We also used several blank (pure air, without odor) control experiments throughout the session to make sure there was no contamination of odors in the odor tube. We used total 11 rats for this study, in that six rats used for orthonasal (16 trials for MV and 12 trails for EB) and five rats used for retronasal (15 trials for MV and 11 trails for EB). Each animal was also anatomically imaged using FLASH (Yang et al., 1998) with a voxel size of 110 × 110 × 250 μm^3. Although we used slightly different voxel sizes and imaging sequences (FLASH vs. EPI, but both gradient-echo contrast with the same TE) in both odor delivery modes, the evoked BOLD activity for the similar odors of same concentration did not significantly differ from each other based on our previously published studies (Sanganahalli et al., 2009, 2016; Thompson et al., 2018).

2.4. Data analysis

Except as indicated, all data analysis was done using custom-written MATLAB (The MathWorks Inc., 2017; www.mathworks.com/products/matlab.html) code. Anatomical images were used co-register between rats. The target of registration was a template created from orthonasal data. Rats 2–6's anatomical images were registered to rat 1's anatomical image using a nonlinear registration (50 iterations, normalized mutual information, and otherwise default) using BioImage Suite (Yale School of Medicine, 2015; bioimagesuite.yale.edu). Then, the average of all six registered images (where data were available) was taken to create a "template" OB image. Anatomical images from all rats, orthonasal and retronasal were then registered to the template using a nonlinear registration (50 iterations, normalized mutual information, and otherwise default) for both orthonasal data and retronasal data. For retronasal data only, both the template and registered anatomical images were masked to only the OB for registration, as positioning was less consistent due to the surgery.

Functional images were co-registered between rats as described in our previous work (Thompson et al., 2018). Slice-timing correction followed by motion-correction (to the middle volume rather than the first volume) was performed in SPM8 (The FIL Methods group, 2015, www.fil.ion.ucl.ac.uk/spm/software/spm8). Following this, the corresponding rat's nonlinear transformation to the template was applied using BioImage Suite (see previous paragraph). To facilitate inter-rat statistics, data were blurred, per-slice, with a Gaussian filter ($\sigma = 2$ voxels/0.250 mm, size = 8 voxels/1 mm). On the template image, masks of the left and right glomerular sheets were drawn by a researcher (BGS).

2.5. Evoked activation maps

Using standard T- or Z-statistics to calculate evoked activation maps would produce biased results between orthonasal and retronasal data sets due to the differing time periods and number of images collected. Therefore, to calculate evoked activation maps we focused on percent change of BOLD (%BOLD) which is relatively consistent for a given contrast and stimulation method. %BOLD was calculated as the mean BOLD during the stimulus period minus the mean of the baseline periods

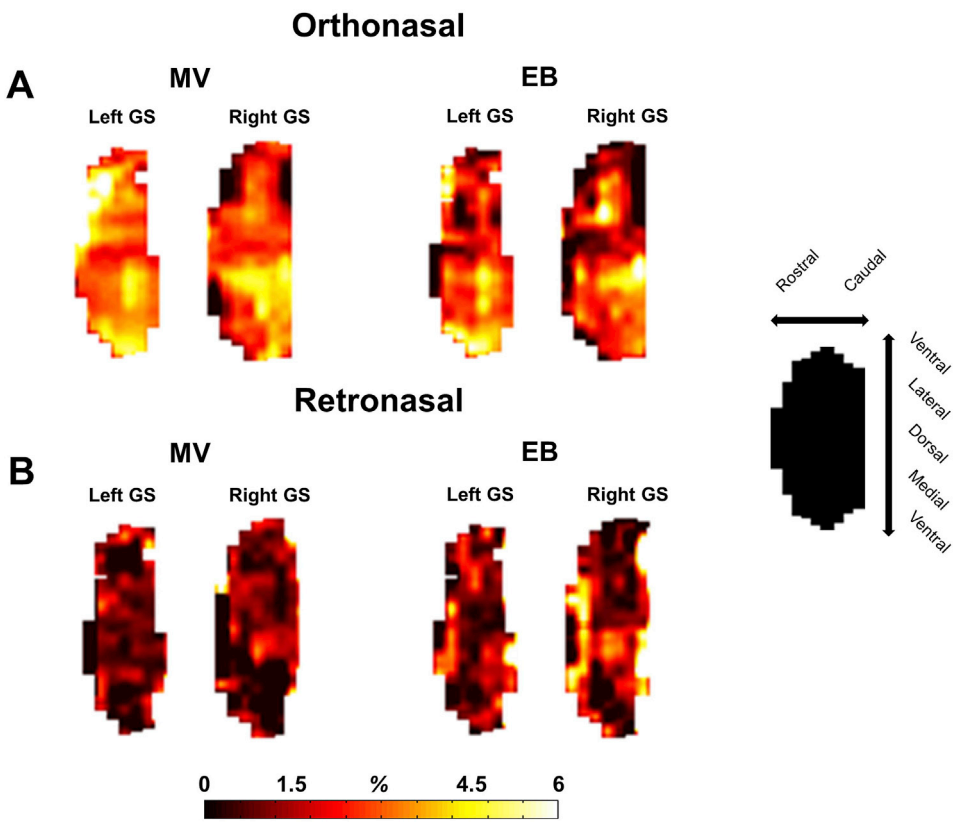

Fig. 2. (A) Glomerular sheet activation for methyl valerate (MV) and ethyl butyrate (EB) odor during orthonasal stimulation (n = 6 rats). Percentage change in fMRI BOLD activation maps was calculated between baseline versus odor stimulation. (B) As A, except retronasal stimulation (n = 5 rats). While all odors are similar (all are esters, fruit-like odors), there are slight differences in the activation patterns between them. Odor concentrations were different for ortho (20%) versus (40%) retronasal stimulation, needed to make BOLD signal amplitudes more similar. Orientation of all flat maps is shown on the right side. Reproducibility maps across trials and subjects were shown in Supplemental Fig. 1.

(prior and succeeding), then divided by the mean of the baseline periods, multiplied by 100%.

For selection of "activated regions" to plot the mean signal over time, only regions within evoked activation maps where %BOLD >0 were taken, and only regions within either the left or right glomerular sheet of each rat. Mean %BOLD was calculated only in these regions, using only the middle half (e.g. start time plus 25th to 75th percentiles of end time) of the activation time period. These steps allowed comparison between the different orthonasal and retronasal modalities without biasing due to differing activation amounts or rise/fall times that may differ between the modalities.

2.6. Comparing orthonasal and retronasal

To test whether there was a difference in total activation percentage, a 3-way ANOVA was calculated on mean %BOLD with each run as a sample and route (orthonasal/retronasal), odor (MV/EB), and side of OB (left/right) as factors. To facilitate comparisons between the spatial extents of orthonasal and retronasal evoked activation patterns, %BOLD within all evoked activation maps had its time-mean subtracted and was subsequently divided by its time-variance on a per-run basis, thus creating a hypothetical normal distribution with zero mean and unit variance, "N(0,1)." To find differences between evoked activation patterns, a two-sample, two-tailed, equal-variance T-test was done in a voxel-wise manner between orthonasal and retronasal runs on a per-odor basis. Resultant p values were corrected for multiple comparisons using sequential goodness of fit (Carvajal-Rodríguez et al., 2009) with separate families for each odor. To find similarities between evoked activation patterns, the mean of all normalized orthonasal evoked activation maps was added to the mean of all normalized retronasal evoked activation maps. As both average maps came from N(0,1) distributions, higher values will occur generally only if both orthonasal and retronasal are locally high. The MATLAB function used for comparing orthonasal and retronasal maps is provided as (script_compare_orthonasal_retronasal_V1.) is provided as supplemental data.

2.7. fMRI visualization of the glomerular sheet

To convert the glomerular sheet from a mask within 3D MRI data to a 2D image, a custom function was written to extract "flatmaps," images of flattened layers in the OB. This function was inspired by OdorMapBuilder (Liu et al., 2004), but is highly simplified. This algorithm is run on 3D data of the OB of any type with a corresponding mask of one layer on one side. Considering the glomerular sheet on each side of the OB as a ring, data within this ring was taken, separated at the bottom, and then considered as a single row with the dorsal bulb in the center and ventral bulb at both ends. Rows for every slice of the image were taken and concatenated, producing a map of one side of the glomerular sheet. This was done for each glomerular sheet (Fig. 1). Following flatmap calculation, the aspect ratio was corrected as slice thickness was greater than in-plane resolution, and a blur (3 × 3 voxel square) was applied to improve visibility. This algorithm is described in detail, including MATLAB code provided for download, was described in more detail in a recent study from our group (Thompson et al., 2018).

2.8. 2-DeoxyGlucose (2-DG) comparison

The z-scored average 2DG map "ethyl butyrate ES3" from the database of Johnson & Leon (Johnson et al., 2005) that was kindly shared with the Verhagen lab was used to compare orthonasal EB responses of the 2-DG modality to that reported by fMRI here. The database did not contain MV. In MATLAB the map (80 × 44 pixels) was converted from a ventral-centered view to the dorsal-centered view used in this study. This was done by flipping the ventral-lateral-dorsal data and separately flipping the ventral-medial-dorsal data, in such a way that the most dorsal edge of the ventral-lateral-dorsal data in original view becomes the midline (row 39) of the new view (Supplementary Fig. 2). Similarly, the ventral-medial-dorsal data was matched to row 40 and onward.

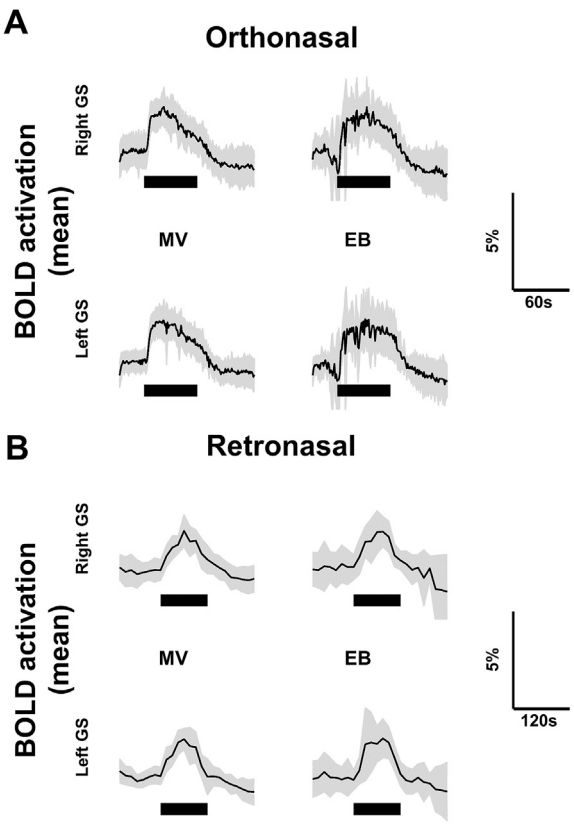

Fig. 3. (A) Activation over time in regions of the left and right bulb's glomerular sheet which have >0% mean activation during stimulation, for the MV and EB odors during orthonasal stimulation. Thin black line is mean of all trials (n = 6 rats), gray shading ±1 S.D., thick black line is time of stimulation. (B) As A, retronasal stimulation (n = 5 rats). Note longer stimulation for retronasal than orthonasal.

3. Results

We investigated the effect of odor route on both spatial and temporal glomerular response patterns in the entire glomerular sheet of the whole OB by fMRI. These results show for the first time the responses of the whole glomerular sheet in any species (here from anesthetized rats) to retronasal odor stimuli, and further compares them to orthonasal odor responses (based on a separate group of rats). The process of converting whole OB 3D MRI data to a flatmap of the glomerular sheet is shown in Fig. 1. The glomerular layer is selected from coronal sections, spliced and laid out along a dorsally-centered sequence at each rostro-caudal level.

The resulting relative change in fMRI BOLD activation maps in the entire glomerular sheet for methyl valerate (MV, a.k.a. methyl pentanoate, $C_6H_{12}O_2$) and ethyl butyrate (EB, a.k.a. ethyl butanoate, butyric ether, $C_6H_{12}O_2$) odors during orthonasal and retronasal stimulation are shown in Fig. 2. We observed reproducible spatio-temporal fMRI activation maps in the glomerular sheet of the whole OB during both orthonasal (n = 6 rats) and retronasal stimuli (n = 5 rats). The reproducibility of maps from different stimulations of the same odor across different trials and subjects are shown in Supplementary Fig. 1. Cross correlation was performed to assess the reproducibility across trials for the left and right OB for the same odor for both orthonasal and retronasal routes (>0.76) whereas for the same odor across orthonasal vs retronasal results were less reproducibile (0.36–0.40). N-way ANOVA determined if the means of data differ with respect to groups of other factors (left OB vs right OB, MV vs EB). No significant difference was observed across bulbs, across odors as well as across routes for the same odor. Odor concentrations were different for orthonasal (20%) versus (40%) retronasal stimuli. The odors are similar in that they both are fruit- smelling esters and accordingly the whole OB response maps also show similar patterns.

In Supplemental Fig. 2 we compare our EB-induced orthonasal BOLD map to the 2-deoxy glucose (2-DG) from the database of Johnson and Leon (Johnson et al., 2005). When the 2DG map is brought to the same dorsally-centered flat map organization the similarities between the maps produced by the two modalities in two different laboratories is striking, particularly with the right BOLD map. Both show large (2DG: z = ~2, BOLD: ~6%) dorso-latero-mid-caudal and dorso-medio-caudal

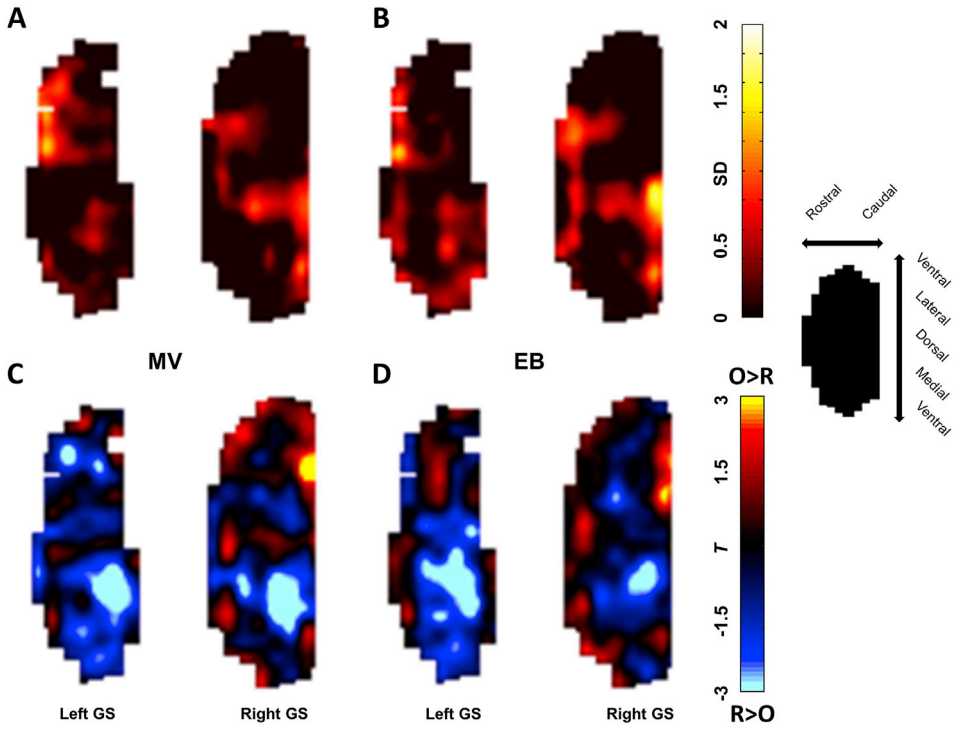

Fig. 4. Statistical maps of differences between orthonasal and retronasal activation patterns. Percent activation maps were normalized on a per-trial basis to zero mean, unit variance. (A) Similarity map. The orthonasal maps for all trials were averaged and summed to the average of the retronasal maps for all trials under MV stimulation. High values indicate co-activation between the two methods. (B) As A, but EB stimulation similarity map. (C) Dominance map. A two-sample, equal-variance, two-tailed T-test was performed between orthonasal trials and retronasal trials for MV stimulation. Resultant T values are shown with orthonasal > retronasal as < 0 (blue) and retronasal > orthonasal as > 0 (red). (D) As C, but EB stimulation dominance map. For both odors, relatively higher activation in the orthonasal condition is seen in dorsal and medial regions, whereas relatively higher activation in the retronasal condition is seen in a small caudal and lateral region. Statistical significance was tested at $p < 0.05$, corrected for multiple comparisons using SGoF, with separate statistical families for each odor. Statistical significance was observed in some regions for both orthonasal > retronasal and retronasal > orthonasal, and also both MV and EB (the spatial extent of statistical significance is shown in Supplemental Fig. 3).

activations.

As expected from prior studies (Gautam and Verhagen, 2012b; Pierce and Halpern, 1996), retronasal stimuli required higher odor concentration (40%) compared to orthonasal delivery (20%) to obtain reproducible fMRI BOLD spatio-temporal activation of similar response amplitudes (Fig. 2). Nonetheless, retronasal maps show larger regions of the glomerular sheet with little or no activation compared to orthonasal route. The dorso-latero-mid-caudal and dorso-medio-caudal activations appear in the OBs for all four conditions, but weaker for the retronasal route, especially for MV-induced activity.

Fig. 3 compares dynamics of BOLD activation in regions of the left and right glomerular sheets for the MV and EB odors during orthonasal and retronasal stimulations (averaged across six rats used for orthonasal (16 trials for MV and 12 trials for EB) and five rats used for retronasal (15 trials for MV and 11 trials for EB)). BOLD time course detrending was not used, as a trend was not observed in the raw data, and detrending would alter the measurement of activation. The mean ± SD of BOLD signal changes for MV and EB during the orthonasal vs. retronasal route are as follows: Ortho-MV: 3.8% ± 1.2%, Ortho-EB: 3.5% ± 1.5%, Retro-MV: 3.5% ± 1.1%, and Retro-EB: 3.7% ± 1.6%. No statistically significant differences between odors and across odor routes were observed. Although we did not find differences in the BOLD signal amplitude, there were significant differences in the temporal delay and shape of the BOLD response curve ($p < 0.02$). Retronasal BOLD time courses showed slower temporal dynamics compared to orthonasal responses. We calculated the area under the curve (AUC) for orthonasal vs retronasal BOLD dynamic responses. AUC for MV and EB for orthonasal/retronasal stimuli were 204 ± 38.67/166 ± 34.54 and 187.8 ± 39.52/154 ± 33.33 respectively. Although the retronasal response curves showed smaller AUC as compared to orthonasal for both odors, they were not statistically significant ($p < 0.4$, unpaired *t*-test) because of the larger response variation.

We next compared the similarity and dominance maps for retronasal and orthonasal stimulations (Fig. 4). Both activations are prominent in the "similarity" maps, based on the sum of z-normalized maps for both routes, for both odors and both bulbs (Fig. 4, top). This confirms coarse response map similarity between the odor routes in the whole OB. We also explored the differences between routes using "dominance" maps, based on t-tests (Fig. 4, bottom). The majority of the glomerular sheet of the whole OB shows strong orthonasal dominance over retronasal responses (blue) to either odor, presumably due to the higher efficacy of the orthonasal route despite double the retronasal odor concentration. This is most pronounced in the dorso-medio-caudal activation common to both odors. Retronasal responses were stronger than orthonasal responses in the most caudal aspect of the lateral OB (in the right OB). Supplemental Fig. 3 shows that these regions are significantly activated.

4. Discussion

We investigated the effect of odor delivery route on both spatial and temporal glomerular response patterns in the entire glomerular sheet of the anesthetized rat OB by fMRI. These results revealed that gross spatial activation patterns are largely independent of stimulus route. As expected based on human psychophysics (Pierce and Halpern, 1996), odor flow modelling (Scott et al., 2014; Zhao et al., 2004), epithelial electrophysiology (Scott et al., 2007a) and dorsal OB optical imaging (Furudono et al., 2013; Gautam et al., 2014; Gautam and Verhagen, 2012b), a higher concentration of odors during retronasal stimulation as compared to orthonasal stimulation was needed to evoke similar whole OB BOLD response amplitudes.

A previous study using calcium imaging found that at a physiologically relevant flow rate, retronasal odorants can effectively reach the olfactory receptor neurons, eliciting glomerular response patterns that grossly overlap with those of orthonasal responses, but differ from the orthonasal patterns in the response amplitude and temporal dynamics (Gautam and Verhagen, 2012b). However, this study and related studies (Furudono et al., 2013; Gautam et al., 2014; Rebello et al., 2015) were optically limited to the dorsal OB.

fMRI BOLD time courses based on the whole OB showed that retronasal responses generally have a longer latency to onset and peak than orthonasal responses. Not only are retronasal fMRI BOLD responses slower to start, but also take more time to reach their peak level relative to this response onset (Fig. 3B). Reported temporal analysis of odorant-evoked (orthonasal) input to the dorsal OB in rodents indicate that odorants can evoke diverse temporal patterns across activated glomeruli in an odorant-specific manner (Junek et al., 2010; Spors and Grinvald, 2002; Spors et al., 2006). This temporal information can then be successfully used by rodents for odor discrimination (Uchida and Mainen, 2003). In addition, modulation of sniff rate can further provide a 'filter' which the animal can use to detect new odors in its environment (Verhagen et al., 2007). Retronasally, the differences in the temporal information of evoked odors allows for the discrimination of ingested mixtures, whereby, differences in solubility of components determines the first odor perceived (Wilkes et al., 2009). Also, the relative timing of a congruent retronasal odor to a drink has been shown to enhance the taste (Kakutani et al., 2017).

Orthonasal and retronasal whole OB fMRI BOLD response spatial activity patterns in general show a large overlap, as well as some dominance for each route (Fig. 4). Orthonasal maps were located more in dorsal-medial regions, whereas retronasal maps were located more in caudal and lateral regions. The spatial maps of odors have been excellently described using 2- DG (Johnson and Leon, 2007a; Johnson et al., 2010). Comparison of the fMRI BOLD orthonasal maps of EB with 2DG confirmed a high degree of similarity between the two maps (Johnson et al., 2005). Previous spatial mapping differences of orthonasal and retronasal odor delivery in the dorsal OB has demonstrated that retronasal maps are subsets of orthonasal maps that are subject to more effective molecular tuning. Long aliphatic chains do not evoke a spatial odor map when delivered retronasally (Kakutani et al., 2017). By imaging the whole OB, the dominance maps highlight that there are differences in the spatial maps of odors based on route in non-dorsal regions of the bulb. Carbon chain length has been shown to shift the spatial maps of odorants away from the dorsal OB to more ventral regions, presumably due to the water solubility of the odorants (Johnson and Leon, 2007a). The more water-soluble odors tend to adsorb to receptors earlier in the nasal cavity. As only the less water soluble odorants are likely to reach the olfactory epithelium when delivered retronasally, it is likely that these also can reach receptors in other areas of the epithelium (Schoenfeld and Cleland, 2005).

In our study we chose to use two ester odors, EB and MV, because they are known to produce relatively similar activation maps with several key differences in medial and lateral regions (Johnson and Leon, 2007a; Thompson et al., 2018). Fig. 4 indicates that many of these lateral odor-specific regions are also coded differently in orthonasal versus retronasal sensing. This underscores that both delivery routes combine with the wide range of odors to create a rich sensory experience. However, other odors that encode highly specific differences in different spatial regions of the OB may instead show greater orthonasal versus retronasal differences in such spatial regions. Nonetheless, as briefly mentioned, we do know that route of odor delivery will affect where odors with different sorption ("water solubility") will bind along the OE (based on the referenced important work of (Mozell, 1964; Scott et al., 2014), which in turn may predict some kind of shift within the OB. However the exact mechanism of this process remains unknown. In fact, our previous study (Gautam and Verhagen, 2012b) found it affected not the spatial pattern, but the temporal pattern (imaged in only the dorsal OB). The much wider field of view of the current whole OB fMRI study thus provides novel insights into route-dependent representations by significantly extending these dorsal OB data. Thus, future work is needed to better understand odor discrimination, especially when comparing highly similar odors to highly different odors in terms of activated regions and behavioral responses.

Could anesthesia differentially affect the OB activations for orthonasal and retronasal pathways? We chose urethane anesthesia for comparing both routes since it is very stable and long lasting anesthetic. How the OB processes, represents, and transmits information of the same olfactory stimulus in different brain states has been systematically investigated using different anesthetics (Li et al., 2011). This study examined both spontaneous and evoked activities in different depths of anesthesia. Regardless of the anesthetic, they found that in two resting-states with rather different spontaneous activities, the levels of peak-evoked activities of the same stimuli did not differ. These results suggest that in the OB, and similarly in other parts of the brain (Hyder and Rothman, 2011), the same peripheral stimulus is represented by a population of neurons with similar total activity levels, independent of the brain states.

These results establish the relationships between orthonasal and retronasal odor representation of the rat whole OB. With appropriate fMRI hardware improvements, we envision the ability to simultaneously image the olfactory bulb and the olfactory cortex to further understand the neurobiological distinctions between orthonasal and retronasal odor delivery routes. This different encoding likely underlies, at least partially, the odor perception for food during ingestion vs. during sniffing. Future experiments measuring the OB and more caudal brain regions simultaneously may reveal how olfactory and other brain regions (like somatosensory cortex) integrate this information. These studies are critical for understanding the perception and neural encoding of food flavor, which is important for feeding behavior and health.

CRediT authorship contribution statement

Basavaraju G. Sanganahalli: Conceptualization, Investigation, Methodology, Formal analysis, Writing - review & editing. **Keeley L. Baker:** Conceptualization, Methodology, Writing - original draft. **Garth J. Thompson:** Investigation, Formal analysis, Software, Data curation. **Peter Herman:** Methodology, Data curation, Resources. **Gordon M. Shepherd:** Conceptualization, Methodology, Validation, Visualization, Supervision. **Justus V. Verhagen:** Conceptualization, Methodology, Formal analysis, Resources, Supervision, Validation, Visualization, Writing - review & editing, Funding acquisition. **Fahmeed Hyder:** Conceptualization, Methodology, Resources, Supervision, Validation, Visualization, Writing - review & editing, Funding acquisition, Project administration.

Acknowledgements

Authors thank Bei Wang for her help in animal preparation for fMRI. Funding for this research included NIH/NIDCD grants R01DC014723 and R01DC011286 and NSF grant IOS-1555880 to JVV and NIH grants R01 MH-067528, P30 NS-052519 to FH. We thank Drs. Michael Leon and Brett A. Johnson for sharing their 2-DG database and allowing this publication of the EB maps based upon it. BGS and GJT thank Dr. Daniel Coman for help with moving code between computer systems and Dr. Elizabeth Lippard for helpful discussions.

Appendix A. Supplementary data

Supplementary data to this article can be found online at https://doi.org/10.1016/j.neuroimage.2020.116664.

References

Blankenship, M.L., Grigorova, M., Katz, D.B., Maier, J.X., 2019. Retronasal odor perception requires taste cortex, but orthonasal does not. Curr. Biol. 29, 62–69 e63.
Bojanowski, V., Hummel, T., 2012. Retronasal perception of odors. Physiol. Behav. 107, 484–487.
Buettner, A., Beer, A., Hannig, C., Settles, M., 2001. Observation of the swallowing process by application of videofluoroscopy and real-time magnetic resonance imaging-consequences for retronasal aroma stimulation. Chem. Senses 26, 1211–1219.
Carvajal-Rodríguez, A., de Uña-Alvarez, J., Rolán-Alvarez, E., 2009. A new multitest correction (SGoF) that increases its statistical power when increasing the number of tests. BMC Bioinformatics 10 (209), 1–14. https://doi.org/10.1186/1471-2105-10-20.
Frasnelli, J., van Ruth, S., Kriukova, I., Hummel, T., 2005. Intranasal concentrations of orally administered flavors. Chem. Senses 30, 575–582.
Furudono, Y., Cruz, G., Lowe, G., 2013. Glomerular input patterns in the mouse olfactory bulb evoked by retronasal odor stimuli. BMC Neurosci. 14, 45-45.
Gautam, S.H., Short, S.M., Verhagen, J.V., 2014. Retronasal odor concentration coding in glomeruli of the rat olfactory bulb. Front. Integr. Neurosci. 8, 81.
Gautam, S.H., Verhagen, J.V., 2010. Evidence that the sweetness of odors depends on experience in rats. Chem. Senses 35, 767–776.
Gautam, S.H., Verhagen, J.V., 2012a. Direct behavioral evidence for retronasal olfaction in rats. PloS One 7, e44781.
Gautam, S.H., Verhagen, J.V., 2012b. Retronasal odor representations in the dorsal olfactory bulb of rats. J. Neurosci. 32, 7949–7959.
Hyder, F., Rothman, D.L., 2011. Evidence for the importance of measuring total brain activity in neuroimaging. Proc. Natl. Acad. Sci. U. S. A. 108, 5475–5476.
Johnson, B.A., Farahbod, H., Saber, S., Leon, M., 2005. Effects of functional group position on spatial representations of aliphatic odorants in the rat olfactory bulb. J. Comp. Neurol. 483, 192–204.
Johnson, B.A., Leon, M., 2000a. Modular representations of odorants in the glomerular layer of the rat olfactory bulb and the effects of stimulus concentration. J. Comp. Neurol. 422, 496–509.
Johnson, B.A., Leon, M., 2000b. Odorant molecular length: one aspect of the olfactory code. J. Comp. Neurol. 426, 330–338.
Johnson, B.A., Leon, M., 2007a. Chemotopic odorant coding in a mammalian olfactory system. J. Comp. Neurol. 503, 1–34.
Johnson, B.A., Ong, J., Leon, M., 2010. Glomerular activity patterns evoked by natural odor objects in the rat olfactory bulb are related to patterns evoked by major odorant components. J. Comp. Neurol. 518, 1542–1555.
Juchem, C., de Graaf, R.A., 2017. B0 magnetic field homogeneity and shimming for in vivo magnetic resonance spectroscopy. Anal. Biochem. 529, 17–29.
Juchem, C., Herman, P., Sanganahalli, B.G., Brown, P.B., McIntyre, S., Nixon, T.W., Green, D., Hyder, F., de Graaf, R.A., 2014. DYNAmic Multi-coil TEchnique (DYNAMITE) shimming of the rat brain at 11.7 T. NMR Biomed. 27, 897–906.
Junek, S., Kludt, E., Wolf, F., Schild, D., 2010. Olfactory coding with patterns of response latencies. Neuron 67, 872–884.
Kakutani, Y., Narumi, T., Kobayakawa, T., Kawai, T., Kusakabe, Y., Kunieda, S., Wada, Y., 2017. Taste of breath: the temporal order of taste and smell synchronized with breathing as a determinant for taste and olfactory integration. Sci. Rep. 7, 8922-8922.
Kent, P.F., Mozell, M.M., Youngentob, S.L., Yurco, P., 2003. Mucosal activity patterns as a basis for olfactory discrimination: comparing behavior and optical recordings. Brain Res. 981, 1–11.
Kida, I., Xu, F., Shulman, R.G., Hyder, F., 2002. Mapping at glomerular resolution: fMRI of rat olfactory bulb. Magn. Reson. Med. 48, 570–576.
Li, A., Gire, D.H., Bozza, T., Restrepo, D., 2014. Precise detection of direct glomerular input duration by the olfactory bulb. J. Neurosci. 34, 16058–16064.
Li, A., Gong, L., Xu, F., 2011. Brain-state-independent neural representation of peripheral stimulation in rat olfactory bulb. Proc. Natl. Acad. Sci. U. S. A. 108, 5087–5092.
Liu, N., Xu, F., Marenco, L., Hyder, F., Miller, P., Shepherd, G.M., 2004. Informatics approaches to functional MRI odor mapping of the rodent olfactory bulb: OdorMapBuilder and OdorMapDB. Neuroinformatics 2, 3–18.
Maier, J.X., 2017. Single-neuron responses to intraoral delivery of odor solutions in primary olfactory and gustatory cortex. J. Neurophysiol. 117, 1293–1304.
Maier, J.X., Wachowiak, M., Katz, D.B., 2012. Chemosensory convergence on primary olfactory cortex. J. Neurosci. 32, 17037–17047.
Mozell, M.M., 1964. Evidence for sorption as a mechanism of the olfactory analysis of vapours. Nature 203, 1181–1182.
Pierce, J., Halpern, B.P., 1996. Orthonasal and retronasal odorant identification based upon vapor phase input from common substances. Chem. Senses 21, 529–543.
Rebello, M.R., Kandukuru, P., Verhagen, J.V., 2015. Direct behavioral and neurophysiological evidence for retronasal olfaction in mice. PloS One 10, e0117218.
Rebello, M.R., McTavish, T.S., Willhite, D.C., Short, S.M., Shepherd, G.M., Verhagen, J.V., 2014. Perception of odors linked to precise timing in the olfactory system. PLoS Biol. 12, e1002021.
Rozin, P., 1982. "Taste-smell confusions" and the duality of the olfactory sense. Percept. Psychophys. 31, 397–401.
Samuelsen, C.L., Fontanini, A., 2017. Processing of intraoral olfactory and gustatory signals in the gustatory cortex of awake rats. J. Neurosci. 37, 244–257.
Sanganahalli, B.G., Bailey, C.J., Herman, P., Hyder, F., 2009. Tactile and non-tactile sensory paradigms for fMRI and neurophysiologic studies in rodents. Methods Mol. Biol. 489, 213–242.
Sanganahalli, B.G., Rebello, M.R., Herman, P., Papademetris, X., Shepherd, G.M., Verhagen, J.V., Hyder, F., 2016. Comparison of glomerular activity patterns by fMRI and wide-field calcium imaging: implications for principles underlying odor mapping. Neuroimage 126, 208–218.
Schafer, J.R., Kida, I., Xu, F., Rothman, D.L., Hyder, F., 2006. Reproducibility of odor maps by fMRI in rodents. Neuroimage 31, 1238–1246.
Schoenfeld, T.A., Cleland, T.A., 2005. The anatomical logic of smell. Trends Neurosci. 28, 620–627.
Scott, J.W., Acevedo, H.P., Sherrill, L., Phan, M., 2007a. Responses of the rat olfactory epithelium to retronasal air flow. J. Neurophysiol. 97, 1941–1950.

Scott, J.W., Sherrill, L., Jiang, J., Zhao, K., 2014. Tuning to odor solubility and sorption pattern in olfactory epithelial responses. J. Neurosci. 34, 2025–2036.
Shusterman, R., Smear, M.C., Koulakov, A.A., Rinberg, D., 2011. Precise olfactory responses tile the sniff cycle. Nat. Neurosci. 14, 1039–1044.
Small, D.M., Gerber, J.C., Mak, Y.E., Hummel, T., 2005. Differential neural responses evoked by orthonasal versus retronasal odorant perception in humans. Neuron 47, 593–605.
Smear, M., Shusterman, R., O'Connor, R., Bozza, T., Rinberg, D., 2011. Perception of sniff phase in mouse olfaction. Nature 479, 397–400.
Spors, H., Grinvald, A., 2002. Spatio-temporal dynamics of odor representations in the mammalian olfactory bulb. Neuron 34, 301–315.
Spors, H., Wachowiak, M., Cohen, L.B., Friedrich, R.W., 2006. Temporal dynamics and latency patterns of receptor neuron input to the olfactory bulb. J. Neurosci. 26, 1247–1259.
Stevenson, R., Boakes, R., Calvert, G., Spence, C., Stein, B., 2004. Sweet and Sour Smells: Learned Synaesthesia between the Senses of Taste and Smell. The Handbook of Multisensory Processing. MIT Press, Cambridge (MA).
Taylor, A.J., Roozen, J.P., 1996. Volatile flavor release from foods during eating. Crit. Rev. Food Sci. Nutr. 36, 765–784.
Thompson, G.J., Sanganahalli, B.G., Baker, K.L., Herman, P., Shepherd, G.M., Verhagen, J.V., Hyder, F., 2018. Spontaneous activity forms a foundation for odor-evoked activation maps in the rat olfactory bulb. Neuroimage 172, 586–596.
Uchida, N., Mainen, Z.F., 2003. Speed and accuracy of olfactory discrimination in the rat. Nat. Neurosci. 6, 1224–1229.
Uchida, N., Takahashi, Y.K., Tanifuji, M., Mori, K., 2000. Odor maps in the mammalian olfactory bulb: domain organization and odorant structural features. Nat. Neurosci. 3, 1035–1043.
Verhagen, J.V., Engelen, L., 2006. The neurocognitive bases of human multimodal food perception: sensory integration. Neurosci. Biobehav. Rev. 30, 613–650.
Verhagen, J.V., Wesson, D.W., Netoff, T.I., White, J.A., Wachowiak, M., 2007. Sniffing controls an adaptive filter of sensory input to the olfactory bulb. Nat. Neurosci. 10, 631.
Wachowiak, M., Cohen, L.B., 2001. Representation of odorants by receptor neuron input to the mouse olfactory bulb. Neuron 32, 723–735.
Wilkes, F.J., Laing, D.G., Hutchinson, I., Jinks, A.L., Monteleone, E., 2009. Temporal processing of olfactory stimuli during retronasal perception. Behav. Brain Res. 200, 68–75.
Xu, F., Kida, I., Hyder, F., Shulman, R.G., 2000. Assessment and discrimination of odor stimuli in rat olfactory bulb by dynamic functional MRI. Proc. Natl. Acad. Sci. U. S. A. 97, 10601–10606.
Xu, F., Liu, N., Kida, I., Rothman, D.L., Hyder, F., Shepherd, G.M., 2003. Odor maps of aldehydes and esters revealed by functional MRI in the glomerular layer of the mouse olfactory bulb. Proc. Natl. Acad. Sci. U. S. A. 100, 11029–11034.
Yang, X., Renken, R., Hyder, F., Siddeek, M., Greer, C.A., Shepherd, G.M., Shulman, R.G., 1998. Dynamic mapping at the laminar level of odor-elicited responses in rat olfactory bulb by functional MRI. Proc. Natl. Acad. Sci. U. S. A. 95, 7715–7720.
Zhao, K., Scherer, P.W., Hajiloo, S.A., Dalton, P., 2004. Effect of anatomy on human nasal air flow and odorant transport patterns: implications for olfaction. Chem. Senses 29, 365–379.